

# PALAIOS, 2023, v. 38, 148–157 Research Article DOI: http://dx.doi.org/10.2110/palo.2021.041



# ONSHORE-OFFSHORE TRENDS IN THE TEMPORAL RESOLUTION OF MOLLUSCAN DEATH ASSEMBLAGES: HOW AGE-FREQUENCY DISTRIBUTIONS REVEAL QUATERNARY SEA-LEVEL HISTORY

MATIAS DO NASCIMENTO RITTER,  $^{1,2}$  FERNANDO ERTHAL,  $^{2,3}$  MATTHEW A. KOSNIK,  $^4$  MICHAŁ KOWALEWSKI,  $^5$  JOÃO CARLOS COIMBRA,  $^{2,3}$  FELIPE CARON,  $^1$  AND DARRELL S. KAUFMAN  $^6$ 

<sup>1</sup>Centro de Estudos Costeiros, Limnológicos e Marinhos, Campus Litoral Norte, Universidade Federal do Rio Grande do Sul, Imbé, RS, CEP 95625-000, Brazil (ORCID: MNR: 0000-0001-8150-4443; FC: 0000-0003-0295-7183)

<sup>2</sup>Programa de Pós-Graduação em Geociências, Instituto de Geociências, Universidade Federal do Rio Grande do Sul, Porto Alegre, RS, CEP 91501-970, Brazil <sup>3</sup>Departamento de Paleontologia e Estratigrafia, Instituto de Geociências, Universidade Federal do Rio Grande do Sul, Porto Alegre, RS, CEP 91501-970, Brazil (ORCID: FE; 0000-0001-8036-192X, JCC: 0000-0002-8980-6531)

<sup>4</sup>School of Natural Sciences, Macquarie University, New South Wales 2109, Australia (ORCID: 0000-0001-5380-7041)
<sup>5</sup>Florida Museum of Natural History, University of Florida, 1659 Museum Road, Gainesville, Florida 32611, USA (ORCID: 0000-0002-8575-4711)
<sup>6</sup>School of Earth and Sustainability, Northern Arizona University, Flagstaff, Arizona, 86011-4099, USA (ORCID: 0000-0002-7572-1414)
email: matias.ritter@ufrgs.br

ABSTRACT: Surficial shell accumulations from shallow marine settings are typically averaged over centennial-to-millennial time scales and dominated by specimens that died in the most recent centuries, resulting in strongly right-skewed age-frequency distributions (AFDs). However, AFDs from modern offshore settings (outer shelf and uppermost continental slope) still need to be explored. Using individually dated shells (\$^{14}\$C-calibrated amino acid racemization), we compared AFDs along an onshore-offshore gradient across the southern Brazilian shelf, with sites ranging from the inner shelf, shallow-water (< 40 m) to offshore, deep-water (> 100 m) settings. The duration of time averaging is slightly higher in deeper water environments, and the AFD shapes change along the depositional profile. The inner shelf AFDs are strongly right-skewed due to the dominance of shells from the most recent millennia (median age range: 0–3 ka). In contrast, on the outer shelf and the uppermost continental slope, AFDs are symmetrical to left-skewed and dominated by specimens that died following the Last Glacial Maximum (median age range: 15–18 ka). The onshore-offshore changes in the observed properties of AFDs—increased median age and decreased skewness, but only slightly increased temporal mixing—likely reflect changes in sea level and concurrent water depth-related changes in biological productivity. These results suggest that on a passive continental margin subject to post-glacial sea-level changes, the magnitude of time-averaging of shell assemblages is less variable along the depositional profile than shell assemblage ages and the shapes of AFDs.

## INTRODUCTION

Water depth, a key parameter of stratigraphic paleobiology, plays an essential role in determining how marine organisms are distributed along an environmental gradient (Holland 1995) as well as how sedimentary processes related to base-level changes influence the resulting fossil record (Patzkowsky and Holland 2012; Scarponi et al. 2013; Shaw et al. 2021). However, in addition to the recognized effect of bathymetry on the paleobiology of accumulations, we also need to understand how the temporal resolution of the marine fossil record relates to water depth.

Temporal mixing of marine shells/skeletal elements determines the temporal resolution of the fossil record and affects the informative value of paleontological data (e.g., Walker and Bambach 1971; Kidwell and Bosence 1991; Kowalewski 1996; Olszewski 1999; Kidwell 2013; Nawrot et al. 2018, 2022; Tomašových et al. 2022). Quantitative estimates of the scale and structure of time averaging of marine invertebrate assemblages have been mainly derived from dating mollusk shells from modern shallow-water marine settings (e.g., Kowalewski et al. 1998; Olszewski and Kaufman 2015; Dominguez et al. 2016; Ritter et al. 2017), although other taxonomic groups and environments are increasingly being examined (e.g., Carroll et al. 2003; Krause et al. 2010; Terry and Novak 2015; Tomašových

et al. 2016; Kowalewski et al. 2018; New et al. 2019; Albano et al. 2020; Nawrot et al. 2022). In shallow marine environments, age-frequency distributions (AFDs) of surficial mollusk or brachiopod shell accumulations tend to be dominated by younger specimens, with rare or no pre-Holocene specimens (e.g., Flessa et al. 1993; Meldahl et al. 1997; Kowalewski et al. 2000; Carroll et al. 2003; Krause et al. 2010; Dexter et al. 2014; Tomašových et al. 2016). However, such right-skewed AFDs may be less common below the sediment interface, reflecting multiple processes that affect accumulations of skeletal remains during the transition from surface to subsurface (Scarponi et al. 2013; Kosnik et al. 2015; Terry and Novak 2015; Dominguez et al. 2016; Tomasovych et al. 2019, 2023). Numerical estimates of time-averaging have also been used to understand how the temporal resolution of the late Quaternary marine fossil record varies at local spatial scales (Dominguez et al. 2016; Ritter et al. 2017), during transgressive-regressive cycles (Scarponi et al. 2013), and as a function of down-core stratigraphic mixing (Kosnik et al. 2015; Dominguez et al. 2016).

However, variation in time-averaging from shallow to deep marine shelf settings has yet to be fully explored. Similarly, estimates of time averaging from deep-water locations are few relative to shallow-water settings, though the work of Tomašových et al. (2016) off the coast of California (89

Published Online: March 2023

Copyright © 2023, SEPM (Society for Sedimentary Geology) 0883-1351/23/038-148

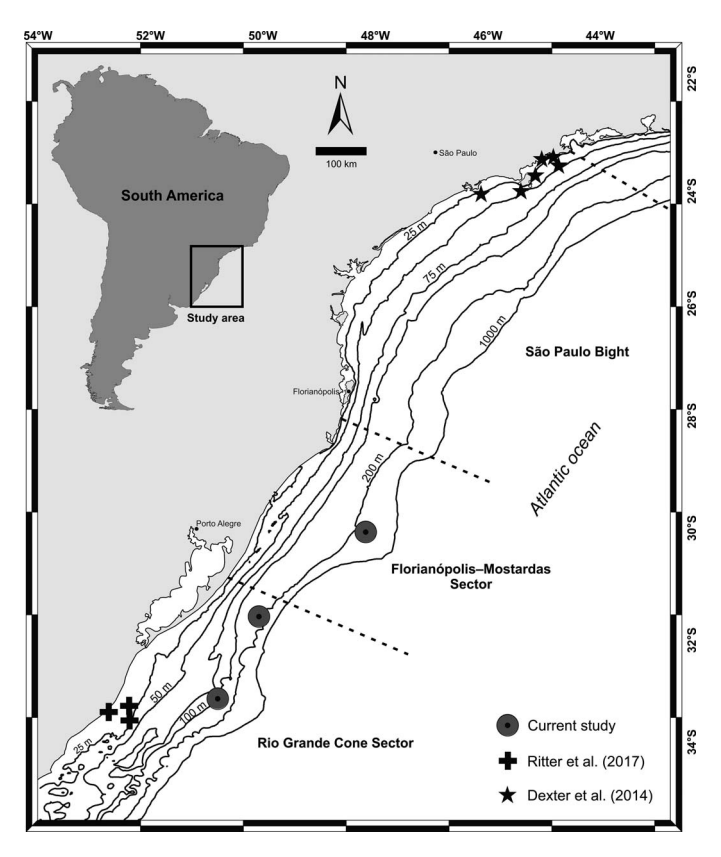


Fig. 1.—Study area and sampling sites on the southern Brazilian shelf (SBS). The SBS sectors (delimited by dashed lines) are based on Zembruscki (1979) and Nagai et al. (2014).

m water depth) is a notable exception. Using individually dated bivalve shells from the southern Brazil shelf (SBS), combined with recalibrated ages from two previously published studies (Dexter et al. 2014; Ritter et al. 2017), we estimate time-averaging along an onshore-offshore depositional profile ranging from sites on the shallow inner shelf (< 40 m water depth) down to the uppermost continental slope (> 100 m water depth).

## MATERIAL AND METHODS

### Study Area

The Southern Brazilian shelf (SBS), a part of the southern Brazilian continental margin, is an Amero-trailing edge coast (Inman and Nordstrom 1971). This subtropical passive margin, which has been tectonically stable over the last glacial cycle, represents one of the widest shelves in the world, varying in width from 100 to 230 km (Fig. 1). The SBS is subdivided into four physiographic sectors (Zembruscki 1979), three of which are included in this study: the São Paulo Bight, the Florianópolis-Mostardas sector, and the Rio Grande Cone sector.

The São Paulo Bight (70–230 km), the northernmost area of the SBS, is the arc-shaped portion of the southern Brazilian margin (Zembruscki 1979), where present-day sedimentation rates are negligible, and late Quaternary sediments are actively being reworked (Mahiques et al. 2011).

The outer shelf margin of the Florianópolis-Mostardas sector corresponds to the most convex part of the SBS due to the influence of the Ponta Grossa arc. This region experienced elevated tectonic activity primarily during the Mesozoic Era (Zembruscki 1979). The Florianópolis-Mostardas area is relatively elevated and irregular, with prominent scarps and mud belts (Mahiques et al. 2011); the width of the continental shelf in this sector varies between 100 and 170 km (Zembruscki 1979). The outer shelf

is dominated by relict biodetrital facies, including mollusks shells, coral fragments, cirriped plates, and foraminiferal tests (Zembruscki 1979; Martins et al. 1985). These deeper shell-rich concentrations—distributed along the SBS shelf break (Martins et al. 1972)—appear similar to shallow water assemblages on the southernmost inner shelf, likely indicating that the deeper assemblages are relicts of the last glacial maximum (LGM), approximately 19–23 thousand years ago, when sea level was roughly 120 m lower than today (Kowsmann et al. 1977; Corrêa 1996). Unlike the Rio Grande Cone sector to the south, the Florianópolis-Mostardas sector has fewer valleys and canyons on the shelf break (Butler 1970; Lopes et al. 2021), possibly enhancing the preservation of surficial shells that have accumulated locally.

In the Rio Grande Cone sector (100–200 km), the present-day continental shelf surface has been interpreted as a subaerial coastal plain developed during the LGM and dissected by fluvial channels before the onset of the postglacial transgression (Weschenfelder et al. 2014). The shelf break, located at water depths between 140 and 180 m, is characterized by the presence of elongated sandbanks and topographical highs with up to 30 m of relief, which may have formed during periods of stable sea level associated with the LGM (Corrêa 1996). In shallow waters, Pleistocene fossiliferous sediments were reworked during the Holocene sea-level rise (Martins et al. 1967; Ritter et al. 2017; Dillenburg et al. 2020).

In the Florianópolis-Mostardas and in the Rio Grande Cone sector, sea level rose at an average rate of 1.2 cm/yr. between  $\sim 20$  ka (the LGM) and 7 ka (Corrêa 1996). At 5.6 ka, during the Middle Holocene, the relative sea level peaked 1–3 m above the present level and subsequently fell slowly until around 4 ka when the rate of relative sea-level fall increased (Angulo et al. 2006; Barboza et al. 2021).

The SBS has been the site of multiple studies focused on time-averaging and its taphonomic, stratigraphic, and eustatic contexts (Carroll et al. 2003; Barbour-Wood et al. 2006; Krause et al. 2010; Dexter et al. 2014; Ritter et al. 2017, 2019; Erthal and Ritter 2020), but those previous studies primarily focused on shallow, inner shelf settings. This study augments those previous analyses by examining a much larger portion of the regional depositional profile to provide a valuable model for understanding stratigraphic paleobiology processes that operate on passive continental margins that experience glacial-interglacial (multi-millennial) scale on sealevel fluctuations.

# Shell Samples

Eighty-six right valves of the shallow infaunal bivalve Saccella larranagai (Klappenbach and Scarabino 1969) (Fig. 2) were dated. Saccella larranagai is a small (< 6 mm), thin-shelled mollusk with a nacreous shell microstructure. It is a deposit-feeder that inhabits offshore soft sediments (mud and sand with high organic content) of the southern South American shelf (Klappenbach and Scarabino 1969). Saccella larranagai is one of the most common species found in the deep waters of the SBS, together with empty shells of Limopsis janeiroensis E.A. Smith 1915, Similipecten nanus (Verrill and J.K. Bush 1897), and Mactra spp. (Amaral and Rossi-Wongtschowski 2004). The Saccella shells were recovered from sediment samples collected from water depths of 100 (n = 25), 160 (n = 31), and 242 m (n = 30). Shells were sampled from the top 10 cm of sediment collected using box cores during the REVIZEE oceanographic project (Living Resources of the Brazilian Economic Exclusive Zone; Amaral and Rossi-Wongtschowski 2004) (22°S to 34°30′S) between April 4th and 15th, 1998.

## Individual Shell Dates

Individual shells were dated using <sup>14</sup>C-calibrated amino acid racemization (AAR). According to the standard procedure (Wehmiller and Miller



Fig. 2.—A right valve of *Saccella larranagai* (Klappenbach and Scarabino 1969). Scale bar = 1 mm

2000), the right valves were prepared for amino acid analysis at Northern Arizona University. The chromatographic instrumentation and procedure used to separate amino acid enantiomers were described by Kaufman and Manley (1998). The ratio of right-hand to left-hand enantiomers (D/L) for all amino acids are reported in the Online Supplementary File (Tables S1, S2). Of the 86 Saccella shells analyzed by AAR, 23 were dated using carbonate target AMS at the Keck Carbon Cycle Accelerator Mass Spectrometry Facility at the University of California Irvine (Bush et al. 2013; Bright et al. 2021) (Online Supplementary File Table S2). Radiocarbon ages were calibrated to calendar years using the marine14 database (Reimer et al. 2013). A regional marine reservoir correction of  $(\Delta R)$  33  $\pm$  24 yr was used based on Angulo et al. (2005). Forty AAR age models were fit using Bayesian model fitting procedures implemented using updated versions of the analytical scripts published by Allen et al. (2013). R packages "rjags" (Plummer 2019), "R2jags" (Su and Yajima 2020), "bbmle" (Bolker and R Core Team 2020), "Hmisc" (Harrell 2020), and "parallelDist" (Eckert 2018) were employed in fitting the age-models and log-likelihood analyses.

Six models had Bayesian Information Criterion (BIC) values within three units of the best-fit model and contributed to the final BIC-weighted average model: two models were fitted to the Asp D/L (D- and L-enantiomers), three models were fitted to Val D/L, and one model was fitted to Phe D/L. Simple power-law kinetics (SPK) functions with empirically fit initial D/L ratios ( $R_0$ ) contributed 75.7% of the BIC weight to the final calibration model. SPK and time-dependent reaction kinetics

(TDK), both with  $R_0=0$ , contributed  $\sim 12\%$  each to the final averaged model (Online Supplementary File Table S3). In addition, models using the gamma (five) and lognormal (one) distributions to estimate uncertainty contributed to the final averaged model.

In addition to the 86 shells dated for this study, the same Bayesian model fitting procedure was used to update the age models for two <sup>14</sup>C-calibrated AAR bivalve datasets: (1) *Semele casali* Doello-Jurado, 1949 from the northern portion of the SBS (São Paulo Bight; Fig. 1) (Barbour Wood et al. 2006; Krause et al. 2010; Dexter et al. 2014; n = 275); and (2) *Mactra isabelleana* d'Orbigny, 1846 from the Rio Grande Cone sector (Fig. 1) (Ritter et al. 2017; n = 60; Online Supplementary File Tables S4–S7). The recalibrated ages allowed us to compare time-averaging estimates between the deep (> 100 m water depth) and shallow areas (< 40 m water depth).

#### Time-Averaging Estimates

Quantifying time-averaging is complicated by the uncertainty associated with estimating specimen age. In a hypothetical situation where all the dated specimens were of identical true age, uncertainty in the specimen age estimates would result in a time-averaging estimate equal to the uncertainty in the age estimates (value greater than the true time-averaging of zero). This straightforward, albeit unlikely, example illustrates that time-averaging estimates must account for age estimation uncertainty. Still, there is yet to be a universally accepted method of addressing dating uncertainty in time-averaging estimates.

One method currently used assumes the total observed variation in an assemblage's age estimate is the sum of the variation due to time-averaging and the variation due to uncertainty in specimen age estimation (Dominguez et al. 2016). This approach to estimating time-averaging uses variation derived from 10,000 Markov-Chain Monte-Carlo (MCMC) replicates to estimate uncertainty (Allen et al. 2013) (for more details, see Allen et al. 2013; Dominguez et al. 2016; Ritter et al. 2017) and partitions the total age variability into two components (Dominguez et al. 2016; Ritter et al. 2017; Kowalewski et al. 2018): (1) time averaging and (2) age estimation error. While Dominguez et al. (2016) used the interquartile range (IQR) to quantify the degree of variability, IQR has been shown to be unreliable in simulation as IQR does not share the same additive properties as variance (Online Supplemental File text and Fig. S1). So, while most of the existing time-averaging literature uses the IQR as the preferred measure of time-averaging, we will use the standard deviation (Tomašových et al. 2023), which has desirable statistical properties (Taylor 1997) and, in simulation, performs well across multiple underlying AFDs (Online Supplemental File text and Fig S1). While the variance is more sensitive to outliers and multi-modal distributions than IQR, variance can be used to account for the age uncertainty, whereas IQR cannot work effectively. We use distinct terminology to avoid confusion with previous studies using IQR. The Estimated Time Averaging (ETA) is computed based on two parametric estimates of dispersion: The Total Assemblage Variance (TAV) and the mean Age Estimation Variance (AEV). The Total Assemblage Variance (TAV) is a sample variance for all the MCMC replicates pooled across all specimens in a sample (Eq. 1):

$$TAV = \frac{\sum_{i=1}^{i=k} (x_i - \bar{x})^2}{k-1}$$
 (Eq. 1)

Where k is the total number of MCMC age estimates combined across all specimens,  $x_i$  is an i<sup>th</sup> MCMC age estimate, and x-bar indicates the grand mean age based on all MCMC age estimates pooled across all specimens. For example, for a sample of 10 specimens, each described by 10,000 MCMC age estimates, TAV is simply a single variance estimated based on all 100,000 MCMC age estimates.

The Age Estimation Variance (AEV) is the mean of variances estimated separately for each specimen based on each specimen's MCMC replicates (Eq. 2):

$$AEV = \frac{1}{n} \sum_{i=1}^{i=n} \frac{\sum_{j=1}^{j=m} (x_{ij} - \bar{x}_i)^2}{m-1}$$
 (Eq. 2)

Where n is the number of specimens included in a sample, m is the number of MCMC estimates for a given specimen,  $x_{ij}$  is a  $j^{\text{th}}$  MCMC age estimate for the  $i^{\text{th}}$  specimen, and  $x_{i^-}bar$  is the mean age of the  $i^{\text{th}}$  specimen. Note that AEV is simply an arithmetic mean of MCMC age variances estimated separately for each specimen and can be considered an estimate of age variation introduced by dating error.

Estimated Time Averaging (ETA) is then defined (Eq. 3) as two times the square root of the Total Assemblage Variance (TAV) minus the mean Age Estimation Variance (AEV):

$$ETA = 2\sqrt{TAV - AEV} = 2\sqrt{\frac{\sum_{i=1}^{i=k} (x_i - \bar{x})^2}{k-1} - \frac{1}{n} \sum_{i=1}^{i=n} \frac{\sum_{j=1}^{j=m} (x_{ij} - \bar{x}_i)^2}{m-1}}{(\text{Eq. 3})}$$

Note that because ETA is computed as a square root of the variance estimate TAV-AEV (Eq. 3), the ETA estimate of time-averaging is in the same units as the original age estimates (years).

The additive property of variance makes it useful for partitioning the uncertainty due to age estimation and age differences due to time averaging. A simulation using typical sample sizes drawn from known parameters (normal, exponential, and uniformly distributed ages using variance to quantify the dispersion of ages) does an excellent job of accounting for age uncertainty in the estimate (Online Supplemental File text and Fig. S1). ETA is analogous to the standard deviation, typically expressed as mean ± SD, where one standard deviation encompasses 34.1% of the area encompassed by a normal distribution. ETA, once multiplied by two, will encompass 68% of a normal distribution's variation (Eq. 3). Since most AFDs are not normally distributed,  $\pm$  SD is unlikely to be 68% of the AFD, but the choice of  $\pm$  SD is no less arbitrary than  $\pm$ 25% represented by IQR. The choice of  $\pm$  SD as a metric for timeaveraging is based on the fact that the math for accounting for age uncertainty is straightforward in theory (Taylor 1997) and practice (Online Supplemental File text). While Tomašových et al. (2023) use the ratio between the observed IQR and the observed SD to estimate a corrected IQR, we found that this approach introduced additional uncertainty in the time-averaging estimate, whereas simply using the square-root of variance (i.e., standard deviation) yields accurate and precise estimates at reasonable sample sizes. While the variance is more sensitive to outliers and multimodal distributions than IOR, variance can be used to account for the age uncertainty, whereas IOR cannot work effectively.

Unfortunately, the metric proposed here (ETA) differs from the existing time-averaging literature. First, ETA is a corrected timeaveraging estimate with the uncertainty due to age estimation removed. All things being equal, this should decrease the estimated amount of time-averaging in an assemblage. Secondly, ETA and IQR are defined to encompass different amounts of the AFD. If the ages are normally distributed, ±1SD or 2SD equates to the inner 68% of the AFD. In contrast, the traditionally used IQR is the inner 50%, so all else being equal, the time-averaging estimates using ETA will be slightly larger than IQR-based time-averaging estimates. For both of these reasons, the two time-averaging metrics should not be directly compared. However, the ETA method effectively removes the effect of dating uncertainty on timeaveraging to yield more accurate and generally smaller time-averaging estimates, especially when age uncertainties are large relative to the magnitude of time-averaging. This approach for removing age uncertainty from the estimated time-averaging does not impact the estimated

The 86 Saccella shells dated here were sampled from three deep-water sites. The 275 Semele dated by Dexter et al. (2014) were sampled from 14 shallow-water sites, and the 60 Mactra dated by Ritter et al. (2017) were

sampled from three shallow-water sites. Time-averaging estimates were calculated for each location. Four sites with < 3 dated *Semele* specimens are excluded due to the small sample size. The skewness and kurtosis of the AFDs were measured using the R package "moments" (Komsta and Novomestky 2015). R scripts (R Core Team 2022) used to implement the analyses and produce the figures are provided in the Online Supplemental File and Ritter et al. (2023).

#### Taphonomic Analysis

Dated shells (Mactra, n = 60 and Saccella, n = 86) were individually scored for quality of preservation using an established taphonomic protocol: shells were examined using a stereoscopic microscope (10× up to 20×) and categorically scored for the extent of encrustation, bioerosion, margin modification, fragmentation, fine-scale surface alteration (outside), and color alteration (summarized in Ritter et al. 2019). Each taphonomic variable was scaled between 0 (pristine) and 1 (maximum taphonomic alteration), making those variables comparable and equally weighted (Ritter et al. 2019). Only individually 14C-dated shells of Semele casali (n = 41 of 275) were included in taphonomic analyses (Dexter et al. 2014; Online Supplemental File Table S9). The median total taphonomic scores (the scores of the cited taphonomic signatures) were calculated separately for each bathymetric category (shallow, n = 101; deep water, n = 86), allowing to test for differences in the state of preservation between environments and species (using Mann-Whitney U pairwise test) and among the three species (using Kruskal-Wallis rank-sum test).

#### RESULTS

## Age and Temporal Resolution

Median shell ages are dramatically older at deeper-water sites (Fig. 3A). The deep-water sites (> 100 m water depth) are dominated by Late Pleistocene shells dated to  $\sim 17$  ka. The shallow-water sites (< 40 m water depth) are dominated by Late Holocene shells dated to  $\sim 0.8$  ka. The 57 m site contains a bimodal mix of two-thirds Holocene shells with a median age of 1.3 ka and one-third Pleistocene shells with a median age of 12.8 ka (Fig. 4I). Time averaging is similarly associated with depth except for a shallow-water *Mactra* assemblage with two  $\sim 39$  ka shells ( $\sim 10\%$  of the sample) resulting in an ETA value of 22 ka (Fig. 3B, Table 1). The deepwater sites have an ETA of  $\sim 6$  ka, the shallow-water sites have an ETA of < 4.4 ka, and the 57 m site has an ETA of 11 ka (Figs. 3B, 4I, Table 1). It is probably a mixture of two age populations of distinctly different ages. However, we cannot exclude the possibility that the intermediate-depth site (57 m) was disturbed by recent seafloor trawling activity (e.g., Cardoso et al. 2021), which could have mixed young and old skeletal biological

Samples from the three deep-water sites are comparable in terms of their assemblage age (16–18 ka) and estimates of time-averaging  $\sim 6$  kyr (Fig. 3). In contrast, the shallow sites yielded consistently young median ages < 3 ka but two assemblages have ETA > 10 kyr versus < 4.4 kyr for all the other shallow water sites (Fig. 3).

The shapes of the assemblage AFDs (based on MCMC replicates including age uncertainty) range from moderately left-skewed to strongly right-skewed, with skewness values ranging from  $g_1 = -3.18$  to 2.70 (Fig. 4). At the same time, the kurtosis values vary from  $g_2 = 1.53$  to  $g_2 = 15.59$ . The deepest sites have the most symmetrical AFDs with very similar mean and median ages (Table 1). The shallowest site has the most skewed AFD due to the presence of  $\sim 10\%$  very old shells. The AFDs are moderately to strongly right-skewed ( $g_1$  range = 0.62–2.70), with a kurtosis range ranging from  $g_2 = 1.53$  to  $g_2 = 12.59$ , indicating variably leptokurtic AFDs (Fig. 4A–4I).

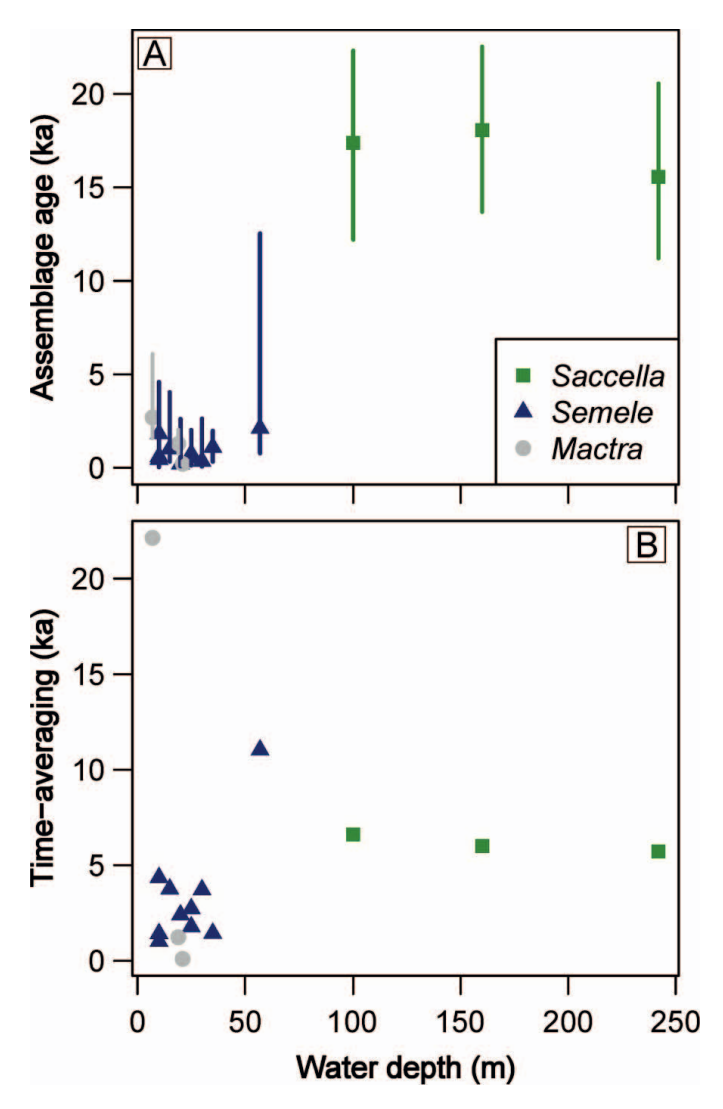


Fig. 3.—Relation between water depth (m) and shell assemblage age parameters (see also Table 1). **A)** Water depth and median assemblage age, with bars indicating the 15.9<sup>th</sup> to 84.1<sup>st</sup> quantiles (one standard deviation) of the age distributions. The increased age variation observed for deeper sites is driven by higher dating uncertainty rather than increased time-averaging. **B)** Water depth and time-averaging accounting for age uncertainty (ETA).

## Taphonomic Bias

Scores indicate that specimens from shallow sites display higher but less variable taphonomic alteration (median = 0.428, IQR = 0.108) than specimens from outer shelf sites (median = 0.321, IQR = 0.154), with a significant difference in terms of taphonomic damage (p = 0.004) (Fig. 5). There is also a difference among species in shallow-water environments (p < 0.001), with *Mactra* having higher taphonomic scores than *Semele*. The taphonomic scores were not significantly different across the three deepwater sites (p = 0.07; Fig. 5).

## TRENDS IN THE TEMPORAL RESOLUTION

After accounting for the uncertainty in estimating shell ages, the scale of time-averaging (ETA) across all sites is weakly related to present-day bathymetry or location along the depositional profile of the SBS. This pattern persists despite sea-level changes: a low stillstand stage associated with the LGM (from before 24 ka to about 15 ka), followed by a relatively

rapid and substantial sea-level rise until 6 ka, then a gentle drop to the current high stillstand. In contrast, the shape of the AFD shifts from right-skewed on the shallow shelf to slightly left-skewed or symmetrical in the distal, modern deep-water settings (Fig. 4). The temporal resolution of this incipient fossil record is lower at offshore sites, with a notable exception of one onshore site and an intermediate-depth site, both of which appear to mix shells from more than one distinctly different population that included very old shells. Trends in the median age and shape of AFDs are much more pronounced than time averaging estimates, likely reflecting processes associated with sea-level rise. Tomašových et al. (2016) noted a similar gradient in time averaging under sea-level rise, with a marked change in AFDs skewness at roughly 51–58 m water depth on the California shelf. Tomašových et al. (2016) also documented a left-skewed distribution at their deepest site (89 m).

In surficial shell accumulations, high biological productivity that typifies mollusks from shallow environments should result in highly right-skewed AFDs (Fig. 4) (e.g., Kidwell 2013), whereas both symmetrical and left-skewed AFDs are expected in regions with reduced shell productivity (e.g., Olszewski and Kaufman 2015; Tomašových et al. 2016). However, shapes of AFD can also be influenced by other factors such as stratigraphic context, boundary conditions of the taphonomically active zone, the dynamics of burial and reworking processes, or a decrease in destruction and sequestration rates below the sediment interface (Olszewski 2004; Scarponi et al. 2013; Olszewski and Kaufman 2015; Terry and Novak 2015; Kosnik et al. 2015; Dominguez et al. 2016; Petro et al. 2018).

In the study system, the changes in the AFDs with depth may be related to changes in shell productivity modulated by the sea-level rise that took place after the LGM. The shoreward shift in the location of the high shell productivity zone over time can account for variations in both median ages and overall shape of AFDs along the depth gradient. This scenario predicts that, during the LGM, water depths at distal shelf-break sites were similar to those found today at shallow sites, with comparably high shell productivity. The post-LGM transgression reduced the shell productivity at those deeper sites and reduced the input of new shells into surficial sediments. The scarcity of shells in age classes younger than  $\sim 15$  ka observed at deeper sites (Figs. 3, 4) is consistent with the suppressed input of new shell material as sea level continued its rise and the offshore sites became progressively deeper. This pattern would reflect the timing of peak productivity as a function of water depth during sea-level rise and does not seem to be related to disintegration and sequestration rates, which were reported to be constant with water depth in other shelf settings (Tomašových et al. 2016).

Although within-bed depositional resolution (= time-averaging) tends to vary as a function of sea-level changes in coastal settings (Scarponi et al. 2013), these temporal trends do not appear to translate into analogous lateral trends. That is, the onshore-offshore trends in the resolution of surficial assemblages across the Brazilian shelf are not analogous to temporal patterns in different parts of a depositional profile (Fig. 3B).

Deep-water sites were continuously submerged during the latest Quaternary, enabling high biological productivity and high shell input during the LGM, when sea level was substantially lower than today. Conversely, present-day shallow-water settings became conducive to high benthic productivity following the Holocene flooding of the proximal shelf (Corrêa 1996). This increase in productivity, coupled with the water-depth oscillations, produced a pattern where median shell ages in shallow-water age assemblages are much younger in AFDs from inner shelf settings, and even the oldest shells tend to be young when compared to deeper water settings ("virgin area" effect of Craig and Oertel 1966; see also Flessa and Kowalewski 1994). The trend toward younger shell ages in proximal parts of the shelf demonstrates that, as a result of sea-level oscillations along siliciclastic passive margins, surficial shell accumulations record increasingly younger time intervals up dip reflecting a landward movement of

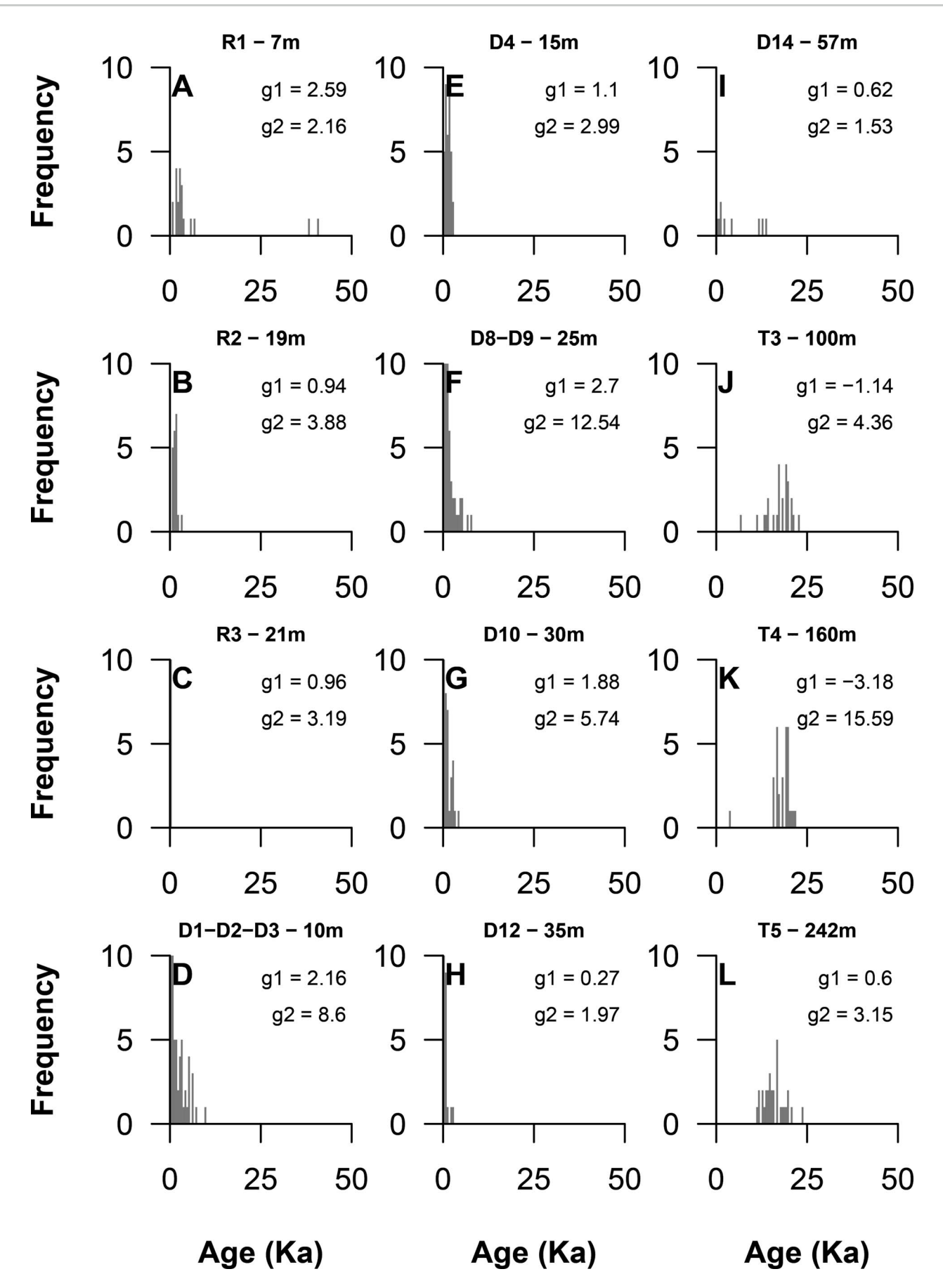


Fig. 4.—Bayesian modeled age-frequency distributions of shell assemblages by collection site (site codes in Table 1; only those sites with n > 8 are displayed here). Sites D1–D14 are from Dexter et al. (2014); sites R1–R3 are from Ritter et al. (2017); sites T3–T5 are the new analyses used here.

Table 1.—Summary of age and time-averaging estimates by site. For each sample, the taxon, number of specimens (N), and water depth are reported (depth). Each sample's mean age, median age, and total age variance (TAV) are based on the sample's combined posterior age distribution. A sample's age-estimation uncertainty (AEV) is the mean-variance of the individual specimen posterior age distributions. The estimated time-averaging (ETA) is two times the square root of TAV - AEV (Eq. 3), and ETA is the preferred measure of time-averaging as it accounts for dating uncertainty and encompasses 68% of the variance of normally distributed data. The interquartile range (IQR) and the standard deviation (SD) of the total age variance are provided for comparison. The sites D1–D14 are those presented in Table 1 of Dexter et al. (2014). The R1–R3 sites are described in Ritter et al. (2017) whereas T3–T5 are new data from this study (see also Fig. 4). Sites with fewer than three shells were not included.

Site	Taxon	N	Depth (m)	Age mean (yrs.)	Age median (yrs.)	TAV (yrs.)	AER (yrs.)	ETA (yrs.)	TAV. IQR (yrs.)	TAV. SD (yrs.)
R1	Mactra isabelleana	20	7	6449	2690	122692317	206174	22134	1905	11077
R2	Mactra isabelleana	20	19	1402	1281	465329	86839	1230	919	682
R3	Mactra isabelleana	20	21	239	211	19235	16928	96	165	139
D1	Semele casali	38	10	2476	1825	4878787	131204	4358	2645	2209
D2	Semele casali	20	10	685	599	275334	16364	1018	767	525
D3	Semele casali	23	10	646	451	515385	10002	1422	857	718
D5	Semele casali	35	15	1855	1012	3572191	45215	3756	2430	1890
D6	Semele casali	4	20	840	206	1443546	1990	2402	643	1201
D8	Semele casali	11	25	798	531	806310	12943	1782	731	898
D9	Semele casali	68	25	1196	738	1883295	24350	2726	1155	1372
D10	Semele casali	37	30	1219	351	3455634	4046	3716	1414	1859
D12	Semele casali	24	35	1186	1100	569333	50582	1440	1136	755
D14	Semele casali	9	57	5378	2110	30598921	176955	11032	9799	5532
T3	Saccella larranagai	25	100	17326	17372	38535475	27611766	6610	6789	6208
T4	Saccella larranagai	31	160	17984	18060	36297699	27288810	6002	5931	6025
T5	Saccella larranagai	30	242	15944	15564	34322818	26154336	5716	6323	5859

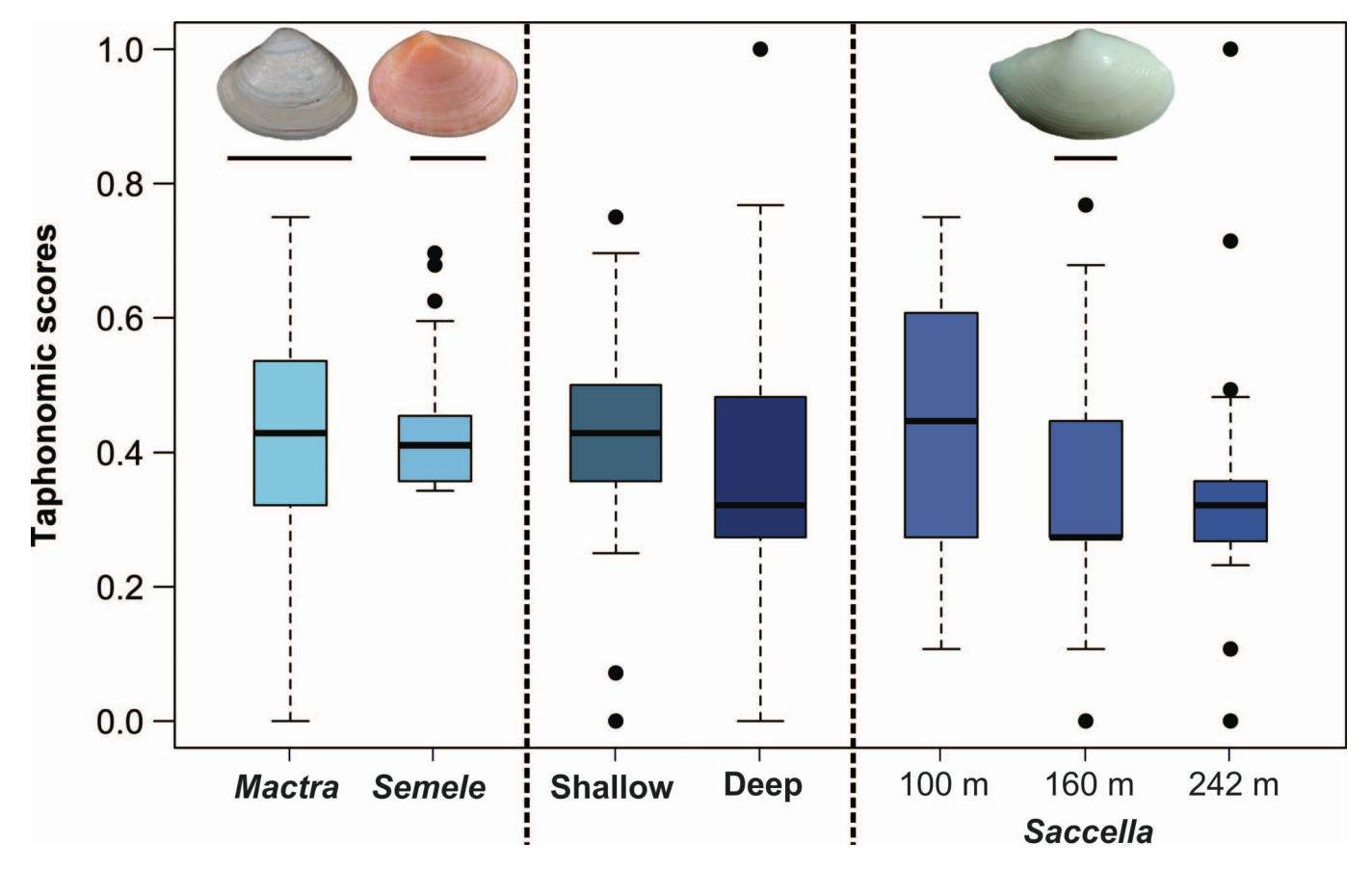


Fig. 5.—Taphonomic scores by species (*Mactra*, *Semele*, and *Saccella*) and assemblage environment (shallow vs. deep). Taphonomic scores are scaled from zero (pristine) to 1 (most altered). The taphonomic scores across shallow sites are for *Mactra* and *Semele* shells, whereas the scores for deep sites are for *Saccella* shells. The *Saccella* shells were grouped by water depth. Shell photo scale bars: *Mactra* and *Semele* =10 mm; *Saccella* = 1 mm.

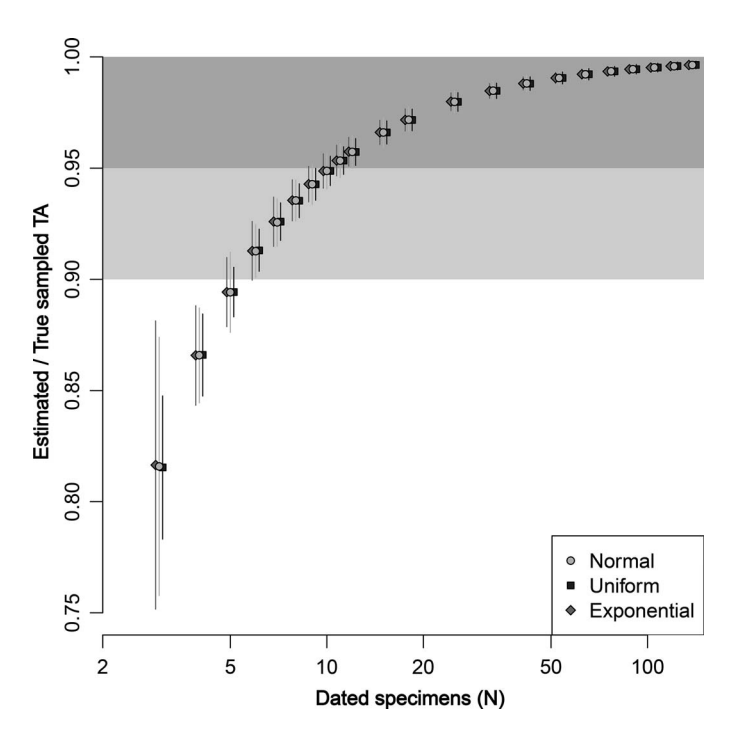


Fig. 6.—The ratio of estimated to true time-averaging for samples with varying numbers of specimens drawn from: normally (gray circle), uniformly (navy blue square), and exponentially (green diamond) distributed age distributions. The uncertainty estimates plotted (vertical lines) are  $\pm 1$  SD for ETA/true sampled time-averaging estimates spanning a range of AEV/TAV estimates (see Online Supplemental File for a detailed description of the simulations). While ETA converges on the true sampled time-averaging at sample sizes of N > 100, at N > 12, the ETA is 96% of the true sampled time-averaging drawn from exponential, normal, or uniform distributions.

highly productive shallow-water habitats concurrent with sea-level rise. Consequently, the dating efforts confirm that surficial shell accumulations located along the shelf edge largely represent relict accumulations from the time when the sea level was much lower (Martins et al. 1967) and record environmental conditions incongruent with their present-day depositional context. As a result, these macrobenthic assemblages are expected to be characterized by elevated live-dead disagreements (e.g., Tomašových and Kidwell 2011). Also, old shells are expected to be transported landward to shallow areas during the Holocene sea-level rise. Our data are more conservative but still agree with Flessa's (1993) estimation: roughly 10% of shells from the shallowest site are much older than expected (~ 40 ka), resulting in a very high time averaging estimate for that sample (Fig. 3B).

Using different species to estimate time-averaging at different sites may have introduced a bias because of potential interspecific differences in shell input and shell disintegration rates (Fig. 5). Whereas the two shallow-water species (*Mactra* and *Semele*) have cross-lamellar shell structures, the offshore species (*Saccella*) possesses a nacreous shell microstructure instead. However, except for one site, the scale of time-averaging does not vary dramatically across sites and taxa, suggesting that those interspecific differences have not played an overriding role in controlling the scale of time-averaging (e.g., Nawrot et al. 2022).

The dating uncertainties (measured in years) increase with specimen age, inflating time-averaging more substantially in samples dominated by older shells (in this case, offshore sites). Most of our individual sites have smaller-than-desirable sample sizes, which could bias the time averaging estimates (Table 1) (see also Olszewski 1999). In a simulation, increasing the number of dated specimens results in estimated time-averaging converging on the true time-averaging of a sample (Fig. 6). Larger sample

sizes reduce the uncertainty in estimates when the AEV/TAV ratio gets larger. Still, for most applications,  $\sim 12$  dates should be sufficient to estimate ETA (Fig. 6). With 12 or more dates, the incremental improvement through dating additional specimens is minimal, and the time-averaging estimated based on a random subset of 12 specimens of a sample is within 5% of the time-averaging estimates based on the whole sample, regardless of the underlying distribution from which the dated specimens were drawn (see Online Supplemental File text for detail of the simulation).

#### CONCLUSION

The results reported here provide empirical estimates of time-averaging and taphonomic patterns in shell assemblages that have accumulated on a passive continental margin during the sea-level rise following the LGM. Analyses of more than 400 individually dated mollusk shells across numerous shallow (< 40 m) and deep-water (> 100 m) sites on the southern Brazilian shelf revealed pronounced differences in the AFDs of surficial shell assemblages. Whereas shallow-water shell assemblages are dominated by individuals from recent millennia and strongly right-skewed AFDs, deep-water shell assemblages are dominated by the latest Pleistocene shells characterized by symmetrical to left-skewed AFDs. The scale of time-averaging also varies, with more pronounced age mixing at offshore sites but these trends are relatively minor when compared to a dramatic offshore increase in shell assemblage ages. The geochronological discrepancies in the AFDs (i.e., differences in median ages and shapes of the curves) most likely reflect sea-level history during the latest Quaternary. Deep-water sites were continuously submerged during the latest Quaternary, enabling temporal mixing even when the sea level was substantially lower than today. However, the input of younger shells into surficial accumulations decreased notably once these sites transitioned to more deep-water settings as sea-level rose. Conversely, shallow-water sites were flooded only in the Holocene, limiting the maximum age of shell availability for mixing ('virgin area effect') and allowing for input of new shell material to continue until the present day.

#### ACKNOWLEDGMENTS

This study was supported by the International Ocean Discovery Program (CAPES/Brazil) (grants 091727/2014, and 010195/2016-02-BEX), the National Council of Technological and Scientific Development (CNPq/MCTI, Brazil) (422766/2018-6), and Jon L. and Beverly A. Thompson Endowment Fund (Florida Museum of Natural History, University of Florida, UFF 013674). The Amino Acid Geochronology Lab is supported by the NSF award 1855381. We also thank John Southon and Katherine Whitacre for their analytical support and Troy Dexter for sharing additional information about his data. The comments of Steven Holland in the first version of this manuscript are also acknowledged. Thomas Olszewski's suggestions substantially improved the final version, especially how we estimate time-averaging and the associated errors, for which we are deeply grateful. An anonymous reviewer also provided insightful comments that improved the quality of this report.

## SUPPLEMENTAL MATERIAL

Data are available online from the PALAIOS Data Archive: https://www.sepm.org/supplemental-materials and from Ritter et al. (2023).

#### REFERENCES

ALBANO, P.G., Hua, Q., Kaufman, D.S., Tomašových, A., Zuschin, M., and Agiadi, K., 2020, Radiocarbon dating supports bivalve-fish age coupling along a bathymetric gradient in high-resolution paleoenvironmental studies: Geology, v. 48, p. 589–593, doi:10.1130/G47210.1.

ALLEN, P.A., KOSNIK, M.A., AND KAUFMAN, D., 2013, Characterizing the dynamics of amino acid racemization using time-dependent reaction kinetics: a Bayesian approach to fitting

- age-calibration models: Quaternary Geochronology, v. 18, p. 63-77, doi: 10.1016/j. quageo.2013.06.003.
- AMARAL, A.C.Z. AND ROSSI-WONGTSCHOWSKI, C.L.D.B., 2004, Biodiversidade bentônica da região Sudeste-Sul do Brasil, plataforma externa e talude superior: São Paulo, Instituto Oceanográfico USP, Série documentos Revizee Score Sul, 216 p.
- ANGULO, R.J., LESSA, G.C., AND SOUZA, M.C, 2006, A critical review of mid- to late-Holocene sea-level fluctuations on the eastern Brazilian coastline: Quaternary Science Reviews, v. 25, p. 486–506, doi: 10.1016/j.quascirev.2005.03.008.
- Angulo, R.J., Souza, M.C., Reimer, P.J., and Sasaoka, S.K., 2005, Reservoir effect of the Southern and Southeastern Brazilian coast: Radiocarbon, v. 47, p. 67–73, doi: 10.1017/S0033822200052206.
- BARBOUR-WOOD, S.L., KRAUSE, JR., R.A., KOWALEWSKI, M., WEHMILLER, J., AND SIMOES, M., 2006, Aspartic acid racemization dating of Holocene brachiopods and bivalves from the southern Brazilian shelf, South Atlantic: Quaternary Research, v. 66, p. 323–331, doi: 10.1016/j.yqres.2006.04.001.
- BARBOZA, E.G., DILLENBURG, S.R., RITTER, M.N., ANGULO, R.J., SILVA, A.B., ROSA, M.L.C., CARON, F., AND SOUZA, M.C., 2021, Holocene sea-level changes in southern Brazil based on high-resolution radar stratigraphy: Geosciences, v. 11, 326, doi: 10.3390/geoscienc es11080326.
- BOLKER, B. AND R DEVELOPMENT CORE TEAM, 2020, bbmle: Tools for General Maximum Likelihood Estimation: R package version 1.0.23.1, https://CRAN.R-project.org/package=bbmle.
- Bright, J., Ebert, C., Kosnik, M.A., Southon, Whitacre, K.J.R., Albano, P., Flores, C., Frazer, T.K., Hua, Q., Kowalewski, M., Martinelli, J.C., Oakley, D., Parker, W.G., Retelle, M., Ritter, M.N., Rivadeneira, M.M., Scarponi, D., Yanes, Y., Zuschin, Z., and Kaufman, D.S., 2021, Comparing direct carbonate and standard graphite <sup>14</sup>C determinations of biogenic carbonates: Radiocarbon, v. 63, p. 387–403, doi: 10.1017/RDC.2020.131.
- Bush, S.L., Santos, G.M., Xu, X., Southon, J.R., Thiagarajan, N., Hines, S.K., and Adkins, J.F., 2013, Simple, rapid, and cost effective: a screening method for <sup>14</sup>C analysis of small carbonate samples: Radiocarbon, v. 55, p. 631–40, doi: 10.2458/azu\_js\_rc.55.1 6192.
- BUTLER, L.W., 1970, Shallow structure of the continental margin, southern Brazil and Uruguay: Geological Society of America Bulletin., v. 81, p. 1079–1096, doi: 10.11 30/0016-7606(1970)81[1079:SSOTCM]2.0.CO;2.
- CARDOSO, L.G., HAIMOVICI, M., ABDALLAH, P.R., SECCHI, E.R., AND KINAS, P.G., 2021, Prevent bottom trawling in southern Brazil: Science, v. 372, p. 138, doi: 10.1126/science. abh0279.
- Carroll, M., Kowalewski, M., Simões, M.G., and Goodfriend, G.A., 2003, Quantitative estimates of time-averaging in brachiopod shell accumulations from a modern tropical shelf: Paleobiology, v. 29, p. 381–402, doi: 10.1666/0094-8373(2003)029<0381: OEOTIT>2.0.CO:2.
- Corrêa, I.C.S., 1996, Les variations du niveau de la mer durant les derniers 17.500 ans BP: l'exemple de la plate-forme continentale du Rio Grande do Sul-Brésil: Marine Geology, v. 130, p. 163–178, doi: 10.1016/0025-3227(95)00126-3.
- CRAIG, G.Y. AND OERTEL, G., 1966, Deterministic models of living and fossil populations of animals: Journal of the Geological Society, v. 122, p. 315–354, doi: 10.1144/gsjgs.1 22.1.0315.
- Dexter, T.A., Kaufman, D.S., Krause, R.A., Jr., Barbour Wood, S.L., Simóes, M.G., Huntley, J.W., Yanes, Y., Romanek, C.S., and Kowalewski, M., 2014, A continuous multi-millennial record of surficial bivalve mollusk shells from the São Paulo Bight, Brazilian shelf: Quaternary Research, v. 81, p. 274–283, doi: 10.1016/j.yqres.2013.12.00 7.
- DILLENBURG, S.R., BARBOZA, E.G., ROSA, M.L.C.C., CARON, F., CANCELLI, R., SANTOS-FISCHER, C.B., LOPES, R.P., AND RITTER, M.N., 2020, Sedimentary records of Marine Isotopic Stage 3 (MIS 3) in southern Brazil: Geo-Marine Letters, v. 40, p. 1099–1108, doi: 10.1007/s00367-019-00574-2.
- DOELLO-JURADO, M., 1949, Dos nuevas especies de bivalvos marinos: Comunicaciones Zoológicas del Museo de Historia Natural de Montevideo, v. 3, p. 1–8.
- D'Orbigny, A.D, 1834–1847, Mollusques, *in* C.P. Bertrand (ed.), Voyage dans l'Amerique Meridionale (Le Bresil, La Republique Orientale de L'Uruguay, La Republique Argentine, La Patagonie, La Republique du Chili, La Republique de Bolivia, La Republique du Perou), execute pendant les annees 1826, 1827, 1828, 1829, 1830, 1831, 1832 et 1833: Chez Ve. Levrault, Paris, Livraison 82, p. 489–528.
- Dominguez, J.G., Kosnik, M.A., Allen, A.P., Hua, Q., Jacob, D.E., Kaufman, D.S., and Whitacre, K., 2016, Time-averaging and stratigraphic resolution in death assemblages and Holocene deposits: Sydney Harbour's molluscan record: PALAIOS, v. 31, p. 563–574, doi: 10.2110/palo.2015.087.
- ECKERT, A., 2018, parallelDist: Parallel Distance Matrix Computation using Multiple Threads: R package version 0.2.4, https://CRAN.R-project.org/package=parallelDist.
- ERTHAL, F. AND RITTER, M.N., 2020, Taphonomy of Recent bioclastic deposits from the southern Brazil shelf: stratigraphic potential, *in* S. Martínez et al. (eds.), Actualistic Taphonomy in South America: Topics in Geobiology, v. 48, p. 1–16, doi:10.1007/978-3-030-20625-3 1.
- FLESSA, K.W., 1993, Well-traveled cockles: shell transport during the Holocene transgression of the southern North Sea: Geology, v. 26, p. 187–190, doi: 10.1130/00 91-7613(1998)026<0187:WTCSTD>2.3.CO;2.

- FLESSA, K.W., CUTLER, A.H., AND MELDAHL, K.H., 1993, Time and taphonomy: quantitative estimates of time-averaging and stratigraphic disorder in a shallow marine habitat: Paleobiology, v. 19, p. 266–286, doi: 10.1017/S0094837300015918.
- FLESSA, K.W. AND KOWALEWSKI, M., 1994, Shell survival and time-averaging in nearshore and shelf environments: estimates from the radiocarbon literature: Lethaia, v. 27, p. 153– 165, doi: 10.1111/j.1502-3931.1994.tb01570.x.
- Harrell Jr., F.E., 2020, Hmisc: Harrell Miscellaneous" R package version 4.4-2, https://CRAN.R-project.org/package=Hmisc.
- HOLLAND, S., 1995, The stratigraphic distribution of fossils: Paleobiology, v. 21, p. 92–109, doi: 10.1017/S0094837300013099.
- Inman, D.L. and Nordstrom, C.E., 1971, On the tectonic and morphologic classification of coasts: Journal of Geology, v. 79, p. 1–21, doi: 10.1086/627583.
- KAUFMAN, D.S. AND MANLEY, W.F., 1998, A new procedure for determining DL amino acid ratios in fossils using reverse-phase liquid chromatography: Quaternary Science Reviews, v. 17, p. 987–1000, doi: 10.1016/S0277-3791(97)00086-3.
- KIDWELL, S.M., 2013, Time-averaging and fidelity of modern death assemblages: building a taphonomic foundation for conservation paleobiology: Palaeontology, v. 56, p. 487–522, doi: 10.1111/pala.12042.
- KIDWELL, S.M. AND BOSENCE, D.W.J., 1991, Taphonomy and time-averaging of marine shelly faunas, *in* P.A. Allison, and D.E.G. Briggs (eds.), Taphonomy: Releasing the Data Locked in the Fossil Record: Plenum, New York, p. 115–209.
- KLAPPENBACH, M.A. AND SCARABINO, V., 1969, Los géneros Nuculana Link, 1807 y Adrana H. and A. Adams, 1858 (Moll. Pelecypoda) en aguas atlánticas sudamericanas, con descripción de una nueva espécie: Revista del Instituto de Investigaciones Pesqueras, v. 2 n. 237–247.
- KOMSTA, L. AND NOVOMESTKY, L., 2015, moments: moments, cumulants, skewness, kurtosis and related tests: R package version 0.14.
- KOSNIK, M.A., HUA, Q., KAUFMAN, D.S., AND ZAWADZKI, A., 2015, Sediment accumulation, stratigraphic order, and the extent of time-averaging in lagoonal sediments: a comparison of <sup>210</sup>Pb and <sup>14</sup>C/amino acid racemization chronologies: Coral Reefs, v. 34, p. 215–229, doi: 10.1007/s00338-014-1234-2.
- KOWALEWSKI, M., 1996, Time-averaging, overcompleteness, and the geological record: The Journal of Geology, v. 104, p. 317–326, doi: 10.1086/629827.
- KOWALEWSKI, M., CASEBOLT, S., HUA, Q., WHITACRE, K.E., KAUFMAN, D.S., AND KOSNIK, M.A., 2018, One fossil record, multiple time resolutions: disparate time-averaging of echinoids and mollusks on a Holocene carbonate platform: Geology, v. 46, p. 51–54, doi: 10.1130/G39789.1.
- KOWALEWSKI, M., GOODFRIEND, G.A., AND FLESSA K.L., 1998, High resolution estimates of temporal mixing within shell beds: the evils and virtues of time-averaging: Paleobiology, v. 24, p. 287–304, doi: 10.1666/0094-8373(1998)024[0287:HEOTMW]2.3.CO;2.
- KOWALEWSKI, M., SERRANO, G.E.A., FLESSA, K.W., AND GOODFRIEND, G.A., 2000, Dead delta's former productivity: two trillion shells at the mouth of the Colorado River: Geology, v. 28, p. 1059–1062, doi: 10.1130/0091-7613(2000)28<1059:DDFPTT>2.0. CO:2
- Kowsmann, R.O., Costa, M.P.A., Vicalvi, M.A., Coutinho, M.G.N., and Gambôa, L.A.P., 1997, Modelo da sedimentação holocênica na plataforma continental sul brasileira: Rio de Janeiro, PETROBRÁS, Projeto REMAC, v. 2, p. 7–26.
- KRAUSE, JR., R.A., BARBOUR, S.L., KOWALEWSKI, M., KAUFMAN, D.S., ROMANEK, C.S., SIMOES, M.G., AND WEHMILLER, J.F., 2010, Quantitative comparisons and models of timeaveraging in bivalve and brachiopod shell accumulations: Paleobiology, v. 36, p. 428– 452, doi: 10.1666/08072.1.
- Lopes, R.P., Bonetti, C., Santos, G.S., Pival, M.A.G., Petró, S.M., Caron, F., and Bonetti, J., 2021, Late Pleistocene sediment accumulation in the lower slope off the Rio Grande terrace, southern Brazilian continental margin: Quaternary International, v. 571, p. 97–116, doi: 10.1016/j.quaint.2020.12.022.
- MAHIQUES, M.M., SOUSA, S.H.M., BURONE, L., NAGAI, R.H., SILVEIRA, I.C.A., FIGUEIRA, R.C.L., SOUTELINO, R.G., PONSONI, L., AND KLEIN, D.A., 2011, Radiocarbon geochronology of the sediments of the São Paulo Bight (southern Brazilian upper margin): Anais da Academia Brasileira de Ciências, v. 83, p. 817–834, doi: 10.1590/S0001-3765201100 5000028.
- MARTINS, L.R., ARIENTI, L.M., MOURA, Y.A., AND SANTOS, N.M., 1985, Contribuição ao estudo da borda da plataforma continental do Rio Grande do Sul: Pesquisas em Geociencias, v. 17, p. 24–44, doi: 10.22456/1807-9806.21688.
- Martins, L.R., Melo, U., França, A.M.C., Santana, C.I., and Martins, I., 1972, Distribuição faciológica da margem continental sulriograndense: Congresso Brasileiro de Geologia, 26, 1972, Belém, Anais, p. 115–132.
- MARTINS, L.R., URIEN, C.M., AND EICHLER, B.B., 1967, Distribuição dos sedimentos modernos da plataforma continental sul-brasileira e uruguaia: Congresso Brasileiro de Geologia, 21st Congress, 1967, Curitiba. Anais, p. 29–43.
- Meldahl, K.H., Flessa, K.W., and Cutler, A.H., 1997, Time-averaging and postmortem skeletal survival in benthic fossil assemblages: quantitative comparisons among Holocene environments: Paleobiology, v. 23, p. 207–229, doi: 10.1017/S00 94837300016791.
- Nagai, R.H., Sousa, S.H.M., and Mahiques, M.M., 2014, The southern Brazilian shelf, *in* F.L. Chiocci and A.R. Chivas (eds.), Continental Shelves of the World: Their Evolution During the Last Glacio-Eustatic Cycle: Geological Society, London, Memoirs 41, p. 47–54 doi: 10.1144/M41.5.

- Nawrot, R., Berensmeier, M., Gallmetzer, I., Haselmair, A., Tomašových, A., and Zuschin, M., 2022, Multiple phyla, one time resolution? Similar time averaging in benthic foraminifera, mollusk, echinoid, crustacean, and otolith fossil assemblages: Geology, v. 50, p. 902–906, doi: 10.1130/G49970.1.
- NAWROT, R., SCARPONI, D., AZZARONE, M., DEXTER, T.A., KUSNERIK, K.M., WITTMER, J.M., AMOROSI, A., AND KOWALEWSKI, M., 2018, Stratigraphic signatures of mass extinctions: ecological and sedimentary determinants: Proceedings of Royal the Society B, v. 285, article 20181191, doi: 10.1098/rspb.2018.119.
- New, E., Yanes, Y., Cameron, R.A.D., Miller, J.H., Teixeira, D., and Kaufman, D.S., 2019, Aminochronology and time averaging of Quaternary land snail assemblages from colluvial deposits in the Madeira Archipelago, Portugal: Quaternary Research, v. 92, p. 483–496. doi: 10.1017/qua.2019.1.
- Olszewski, T., 1999, Taking advantage of time-averaging: Paleobiology, v. 25, p. 226–238, doi: 10.1017/S009483730002652X.
- OLSZEWSKI, T.D., 2004, Modeling the influence of taphonomic destruction, reworking, and burial on time-averaging in fossil accumulations: PALAIOS, v. 19, p. 39–50, doi: 10.1 669/0883-1351(2004)019<0039:MTIOTD>2.0.CO;2.
- OLSZEWSKI, T.D. AND KAUFMAN, D.S., 2015, Tracing burial history and sediment recycling in an estuarine bay (Copano Bay, Texas) using postmortem ages of the bivalve *Mulinia lateralis*: PALAIOS, v. 30, p. 224–237, doi: 10.2110/palo.2014.063.
- PATZKOWSKY, M.E. AND HOLLAND, S.M., 2012, Stratigraphic Paleobiology: Understanding the Distribution of Fossil Taxa in Time and Space: University of Chicago Press, Chicago, 259 p.
- PETRÓ, S.M., RITTER, M.N., PIVEL, M.A.G., AND COIMBRA, J.C., 2018, Surviving in the water column: defining the taphonomically active zone in pelagic systems: PALAIOS, v. 33, p. 85–93, doi: 10.2110/palo.2017.032.
- PLUMMER, M., 2019, rjags: Bayesian Graphical Models using MCMC, R package version 4-10, https://CRAN.R-project.org/package=rjags.
- R Core Team, 2020, R: A language and environment for statistical computing: R Foundation for Statistical Computing, Vienna, www.R-project.org.
- REIMER, P.J., BARD, E., BAYLISS, A., BECK, J.W., BLACKWELL, P.G., RAMSEY, B.C., BUCK, C.E., CHENG, H., EDWARDS, R.L., FRIEDRICH, M., GROOTES, P.M., GUILDERSON, T.P., HAFLIDASON, H., HAJDAS, I., HATTÉ, C., HEATON, T.J., HOFFMANN, D.L., HOGG, A.G., HUGHEN, K.A., KAISER, K.F., KROMER, B., MANNING, S.W., NIU, M., REIMER, R.W., RICHARDS, D.A., SCOTT, E.M., SOUTHON, J.R, STAFF, R.A., TURNEY, C.S.M., AND VAN DER PLICHT, J., 2013, IntCal13 and Marine13 radiocarbon age calibration curves 0–50,000 years cal BP: Radiocarbon, v. 55, p. 1869–1887, doi: 10.2458/azu\_js\_rc.55.16947.
- RITTER, M.N., ERTHAL, F., AND COIMBRA, J.C. 2019, Depth as an overarching environmental variable that modulates the preservation potential and temporal resolution of shelly taphofacies: Lethaia, v. 52, p. 44–56, doi: 10.1111/let.12289.
- RITTER, M.N., ERTHAL, F., KOSNIK, M.A., COIMBRA, J.C., AND KAUFMAN, D.S. 2017, Spatial variation in the temporal resolution of subtropical shallow-water molluscan death assemblages: PALAIOS, v. 32, p. 559–571, doi: 10.2110/palo.2017.003.
- RITTER, M.N., ERTHAL, F., KOSNIK, M.A., KOWALEWSKI, M., COIMBRA, J.C., CARON, F., AND KAUFMAN, D.S., 2023, Supplementary material: onshore-offshore trends in the temporal resolution of molluscan death assemblages: how age-frequency distributions reveal Quaternary sea-level history: Figshare, doi: 10.6084/m9.figshare.20220171.
- SCARPONI, D., KAUFMAN, D.S., AMOROSI, A., AND KOWALEWSKI, M., 2013, Sequence stratigraphy and the resolution of the fossil record: Geology, v. 41, p. 239–242, doi: 10.1130/G33849.1.

- SHAW, J.O., BRIGGS, D.E.G., AND HULL, P.M., 2021, Fossilization potential of marine assemblages and environments: Geology, v. 49, p. 258–262, doi: 10.1130/G47907.1.
- SMITH, E.A., 1915, Mollusca, Part I, Gastropoda Prosobranchia, Scaphopoda, and Pelecypoda: London, British Antarctic ("Terra Nova") Expedition, 1910, British Museum (Natural History), Natural History Report, Zoology, v. 2, p. 61–112.
- Su, Y-S. and Yajima, M., 2020, R2jags: using R to Run 'JAGS': R package version 0.6-1, https://CRAN.R-project.org/package=R2jags.
- Taylor, R.E., 1997, Radiocarbon dating, *in R.E.* Taylor and M.J. Aitken (eds.), Chronometric Dating in Archaeology: Plenum Press, New York, p. 65–96.
- Terry, R.C. and Novak, M., 2015, Where does the time go?: Mixing and the depth-dependent distribution of fossil ages: Geology, v. 43, p. 487–490, doi: 10.1130/G36483.1.
- Tomašových, A., Gallmetzer, I., Haselmair, A., and Zuschin, M., 2022, Inferring time averaging and hiatus durations in the stratigraphic record of high-frequency depositional sequences: Sedimentology, v. 69, p. 1083–1118, doi: 10.1111/sed.12936.
- Tomašových, A. and Kidwell, S.M., 2011, Accounting for the effects of biological variability and temporal autocorrelation in assessing the preservation of species abundance: Paleobiology, v. 37, p. 332–354, doi: 10.1666/09506.1.
- TOMAŠOVÝCH, A., KIDWELL, S.M., ALEXANDER, C.R., AND KAUFMAN, D.S., 2019, Millennial-scale age offsets within fossil assemblages: result of bioturbation below the taphonomic active zone and out-of-phase production: Paleoceanography and Paleoclimatology, v. 34, p. 954–977, doi: 10.1029/2018PA003553.
- Tomašových, A., Kidwell, S.M., and Barber, R.F., 2016, Inferring skeletal production from time-averaged assemblages: skeletal loss pulls the timing of production pulses towards the modern period: Paleobiology, v. 42, p. 54–76, doi: 10.1017/pab.2015.30.
- Tomašových, A., Kidwell, S.M., Barber, R.F., and Kaufman, D.S., 2016, Long-term accumulation of carbonate shells reflects a 100-fold drop in loss rate: Geology, v. 42, p. 819–822, doi: 10.1130/G35694.1.
- Tomašových, A., Kidwell, S.M., and Dai, R., 2023, Modeling the transition of death assemblages through the mixed layer predicts a downcore increase in time averaging. Paleobiology, doi: 10.1017/pab.2021.62.
- VERRILL, A.E., 1897, A study of the family Pectinidae, with a revision of the genera and subgenera: Transactions of the Connecticut Academy of Arts and Sciences, v. 10, p. 41– 95.
- Walker, K.R. and Bambach, R.K., 1971, The significance of fossil assemblages from fine grained sediments: time-averaged communities: Geological Society of America Annual Meeting Program with Abstracts, v. 3, p. 783–784.
- Wehmiller, J.F. and Miller, G.H., 2000, Aminostratigraphic dating methods in Quaternary Geology, *in J.S.* Noller, J.M. Sowers, and W.R. Lettis (eds.), Quaternary geochronology: Methods and Applications: American Geophysical Union Reference Shelf Series, v. 4, Washington, DC, p. 187–222, doi: 10.1029/RF004p0187.
- Weschenfelder, J., Baitelli, R., Corréa, I.C.S., Bortolin, E.C., and Santos, C.B., 2014, Quaternary incised valleys in southern Brazil coastal zone: Journal of South American Earth Sciences, v. 55, p. 83–93, doi: 10.1016/j.jsames.2014.07.004.
- Zembruscki, S.G., 1979, Geomorfologia da margem continental sul brasileira e das bacias oceânicas adjacentes, *in* H.A.F. Chaves (ed.), Geomorfologia da margem continental brasileira e das bacias oceânicas adjacentes: Rio de Janeiro, PETROBRAS, ENPES, DINTEP, Projeto REMAC Series 7, p. 129–177.

Received 20 August 2021; accepted 27 February 2023.